Understanding the Effects of Bi Modification on the Properties of Ni-rich Cathodes

Zifei Meng, Jiahui Hou, Panya Thanwisai, Jinzhao Fu, Zeyi Yao, Yadong Zheng, Wenting Jin, Zexin Wang, Zhenzhen Yang, Xiaotu Ma, Yan Wang**

Z. Meng, J. Hou, P. Thanwisai, J. Fu, Z. Yao, Y. Zheng, W. Jin, Z. Wang, X. Ma, Y. Wang.

Department of Mechanical and Materials Engineering, Worcester Polytechnic Institute,

Worcester, MA 01609, USA

E-mail: xma3@wpi.edu

E-mail: yanwang@wpi.edu

Z. Yang

Chemical Sciences and Engineering Division, Argonne National Laboratory, Lemont, IL

60439, USA

Keywords

Lithium-ion battery, Ni-rich cathode materials, Bi modification, structural stability

Abstract

With the skyrocketing market demands for energy storage, lithium ions batteries (LIB) with higher energy density are urgently needed. Cathodes play a critical role in determining the energy density of LIB, and the most popular one is Ni-rich cathode due to its high capacity. However, due to the fast structural degradation, Ni-rich cathode materials should be further modified to achieve higher stability. Herein, we introduce bismuth ions in $LiNi_{0.83}Co_{0.11}Mn_{0.06}O_2$ cathodes by adding Bi_2O_3 during sintering to optimize the specific capacity and cycle stability. By adding 0.1% mol Bi, the Li^+ diffusion and structural stability are effectively optimized, leading to improved electrochemical performances. The modified sample delivers much higher specific capacity (222.9 $mAhg^{-1}$, 0.05C) than unmodified sample (204 $mAhg^{-1}$, 0.05C). Meanwhile, the specific capacity of optimized sample after 100 cycles at 0.33C is 27.75 $mAhg^{-1}$ higher than that of unmodified sample. Therefore, this work demonstrates that Bi modification can be regarded as a possible solution to optimizing the electrochemical performance of Ni-rich cathodes.

1. Introduction

The skyrocketing demands of LIB is motivated by the popularity of electric vehicles during recent decades due to the high energy density of LIB.[1] To meet the rapid growing of the requirement for energy storage, the performance of LIB should be further improved. Cathode materials can significantly influence the energy and power density of LIB, acting as the major performance-limiting factor.[2] Many cathode materials have been developed, such as Ni-rich, Mn-rich and Li-rich oxide materials.[3-5] However, these cathode materials often face fading issues, like structure degradation. [6-8] The structure degradation is mainly caused by the structure collapse and the irreversible phase transition during lithiation/delithiation process, leading to fast capacity fading. [9-11] Meanwhile, the poor stability of structure can also cause low capacity at high rates. [12, 13] Therefore, the structure stability of cathode materials is emergent to be optimized. [14, 15] Different modification strategies have been employed to improve the structure stability, like controlling the exposed facets and morphology of primary particles, optimizing the solid electrolyte interphase (SEI), and synthesizing single crystal shapes. [16-18]

Doping and coating are the most popular modification strategies because they are significantly effective and can be simply achieved during synthesis process. [19-21] Zhou et al. proposed that Bi_2O_3 at surface can hinder the migration of oxygen ion vacancies and reduce the irreversible loss of oxygen and thus optimize the structure stability and improve Li^+ diffusion of $Li_{1.2}Mn_{0.54}Ni_{0.13}Co_{0.13}O_2$, achieving high cycle and rate capability.[22] Hao et al. also claimed that Bi ions can optimize the interfacial stability. With 0.07 mol% Bi doping, the capacity and cyclability of LMO can be optimized, and the capacity retention of Bi modified sample is 54.3 $mAhg^{-1}$ higher than that of unmodified sample.[23] However, Bi_2O_3 has not been employed as a dopant in polycrystal Ni-rich cathode materials to improve the electrochemical performance. $Bi(NO_3)_3$ has only been used to optimize the synthesis process of single crystal $LiNi_{0.6}Co_{0.2}Mn_{0.2}O_2$, and Bi ions can lower the sintering temperature because Bi ions gather at

the gain boundary and accelerate the diffusion and fusion of primary particles during synthesis process. However, the specific capacity of Bi modified samples are much lower than that of unmodified sample.[24] Therefore, whether Bi_2O_3 can be regarded as possible doping or coating materials to optimize the properties of Ni-rich cathode materials is still unclear.

Herein, in this study, we study the impacts of Bi substitution on the crystal structure and electrochemical performance of the Ni-rich cathodes. By introducing Bi ions, the electrochemical performance of NMC cathode materials has been significantly improved. Especially for the NMC cathode modified with 0.1 mol% Bi (1BiNMC), it delivers the best electrochemical performance in both rate and cycling tests. The specific capacity of 1BiNMC at 0.05C is 18.9 $mAhg^{-1}$ higher than VNMC and with higher rate, 5C, it is 43.4 $mAhg^{-1}$ higher than VNMC. Meanwhile, the capacity retention of 1BiNMC is 87.44% after 100 cycles at 0.33C, ~10% higher than VNMC. As revealed by various characterizations, Bi substitution can not only lower the cation mixing but also can limit contraction in c-direction to reinforce structural stability and prevent the formation of cracks. Altogether, our work demonstrates that Bi modification can be regarded as a possible solution to optimizing the electrochemical performance of Ni-rich cathodes.

2. Results and discussions

2.1. Morphology and Crystallinity

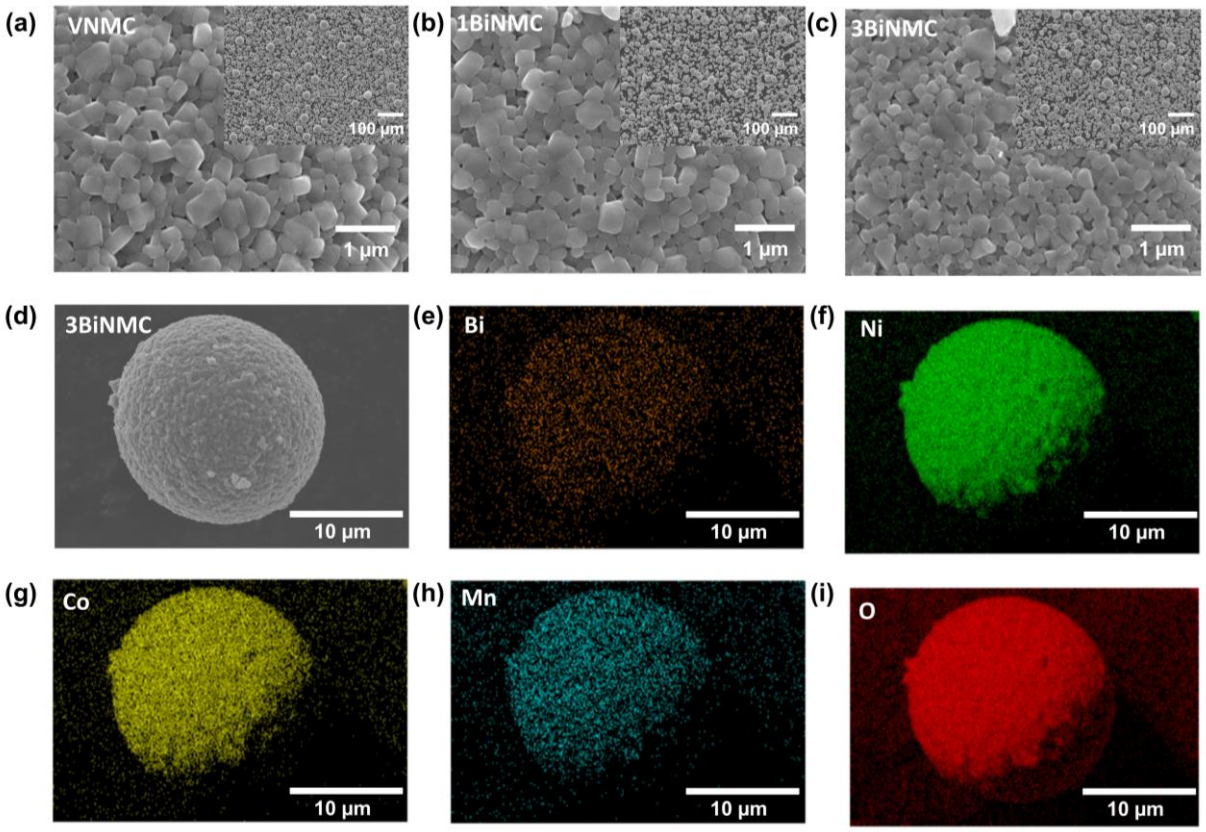

Fig.1. M**orphology and elemental distribution of VNMC, 1BiNMC, and 3BiNMC.** (a-c) SEM image of VNMC, 1BiNMC, and 3BiNMC; (d-i) EDX mappings image of 3BiNMC; The inset in (a) presents the low magnification SEM image of VNMC; The inset in (b) presents the low magnification SEM image of 1BiNMC; The inset in (c) presents the low magnification SEM image of 3BiNMC.

The morphology of VNMC, 1BiNMC, and 3BiNMC are observed through SEM, as shown in Fig. a-c. Secondary particles in all samples are spheres and the particle size distribution of all samples are similar. However, the difference in the primary particle size among the three samples is obvious, and the primary particle size decreases with higher concentration of Bi ions. The primary particle size of VNMC is around 300 nm. For 1BiNMC, the primary particles are almost 250 nm with a little 300nm particles. In 3BiNMC, the primary particles are around

150nm, much less than that of VNMC and 1BiNMC. The chemical bonds between Bi and nonmetals are stronger than those in NMC and when Bi ions were added during synthesizing NMC and diffuse into the precursors, they can suppress the growth of primary particles in the precursor and cause small primary particles in the obtained cathode materials.[25] Thus, for 1BiNMC, the primary particle size is only around 50 nm smaller than VNMC while for 3BiNMC, the primary particle size is around half of that in VNMC. The smaller primary particles can reduce the Li^+ diffusion path length and lead to a denser stacking structure, which helps prevent the breakdown of secondary particles.[25] The elemental distribution of VNMC, 1BiNMC, and 3BiNMC is examined by the EDX mapping. The particle microstructure of VNMC and 1BiNMC is investigated by cross-sectional SEM, as shown in Fig.S1. Primary particles in VNMC are randomly oriented while for 1BiNMC, primary particles tend to be radially oriented. The radial orientation of primary particles allows short Li^+ diffusion path from bulk to surface in secondary particles, enabling higher diffusion coefficient and better rate performance. In Fig.1d-i, S2 and S3, Ni, Mn, Co, and O elements are distributed uniformly in all samples. Meanwhile, the uniform distribution of Bi on 3BiNMC can be observed in Fig.1e.

2.2. Composition and Structure

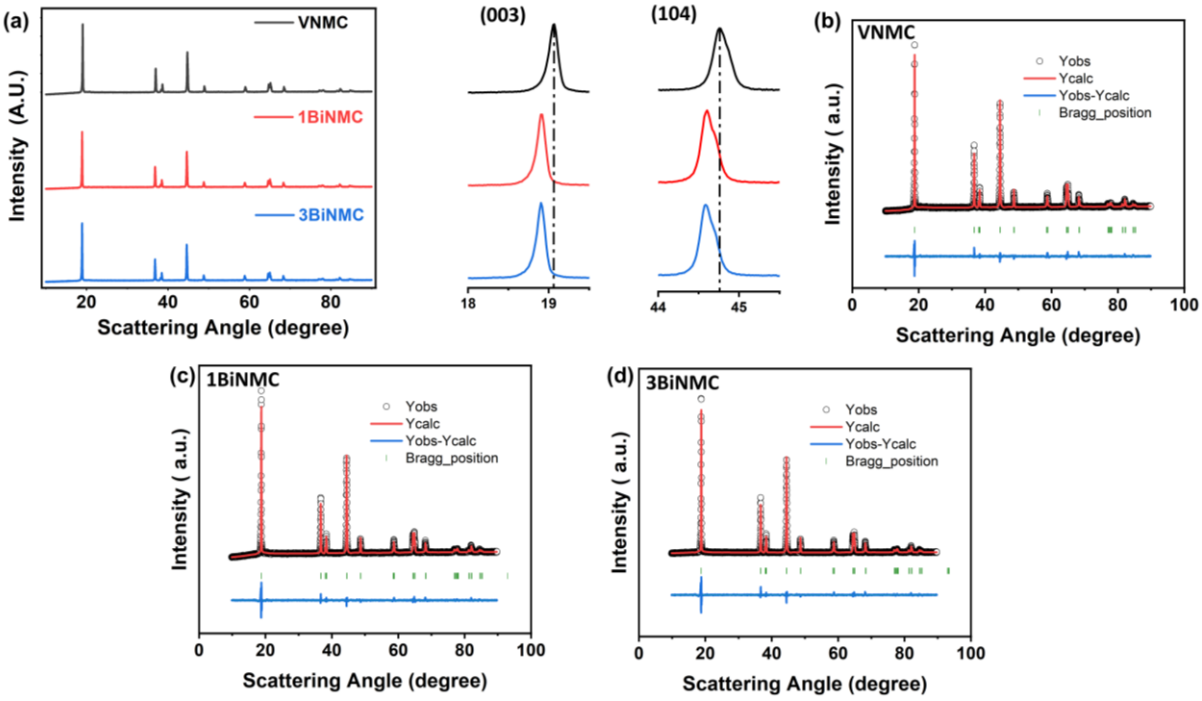

Fig.2. **The structure information of VNMC, 1BiNMC, and 3BiNMC.** (a) X-ray diffraction patterns and their (003) and (104) planes of VNMC, 1BiNMC, and 3BiNMC; (b-d) Refinement profile of VNMC, 1BiNMC, and 3BiNMC.

Table 1. Refinement data of VNMC, 1BiNMC, and 3BiNMC.

Sample	**a/b-axis (Å)**	**c-axis (Å)**	**Volume (Å^3)**	**Ni in Li layer (%)**	**χ^2**	**Rwp (%)**
VNMC	2.8709	14.1941	101.312	4.76%	5.67	2.72
1BiNMC	2.8730	14.2030	101.528	4.49%	5.09	2.60
3BiNMC	2.8761	14.2184	101.858	4.55%	7.50	5.48

The results of ICP-MS indicate that the Bi modified NMC cathodes were synthesized successfully with the desired composition (Table S1). The percentage of Mn and Co matches the designed composition while only the percentage of Ni ions decreases with the increasing

percentage of Bi ions, indicating that the sites of Ni ions were occupied by Bi ions. Meanwhile, according to the XRD results in Fig.2a, there are no impurity phases and the clear splitting of (108)/(110) and (006)/(102) peaks indicates the well crystalline layered structure of all samples. [26, 27] However, because the radius of Bi ions are larger than that of other transition metal ions, Bi ions are able to cause lattice expansion.[28] In Fig.2a, the (003) and (104) peaks of Bi modified NMC cathodes shift to the left, indicating the lattice expansion in 1BiNMC and 3BiNMC. [29, 30] The corresponding lattice expansion is also investigated by the XRD refinement results in Fig.2b-d and Table.1. The expansion of lattice can broad the Li^+ diffusion path, causing faster Li^+ diffusion and better rate performance.[31] The cation mixing in the Li layer also can be obtained from the XRD refinement results, and cation mixing of 1BiNMC and 3BiNMC are 4.49% and 4.55%, respectively. Both of them have lower cation mixing than VNMC(4.76%), which representing the highly ordered layered structure.[29] Because of the low cation mixing and highly ordered layered structure, optimized specific capacity and cycle stability can be achieved. [32]

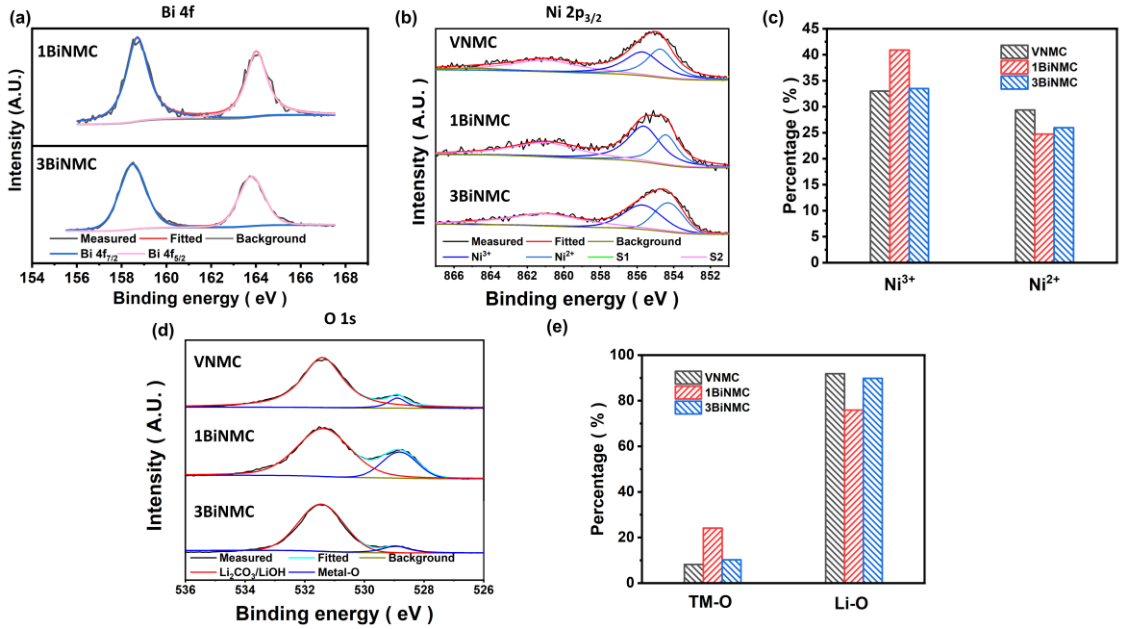

Fig.3. **The surface chemical states of elements in VNMC, 1BiNMC, and 3BiNMC.** (a) High-resolution XPS spectra of Bi 4f in 1BiNMC, and 3BiNMC; (b) High-resolution XPS spectra of Ni $2p_{3/2}$ in VNMC, 1BiNMC, and 3BiNMC; (c) Percentage of Ni^{2+} and Ni^{3+} ions in VNMC,

1BiNMC, and 3BiNMC; (d) High-resolution XPS spectra of O 1s in VNMC, 1BiNMC, and 3BiNMC; (e) Percentage of peaks of O 1s in VNMC, 1BiNMC, and 3BiNMC.

To determine the functions of Bi ions on the surface chemical states of NMC, the high-resolution XPS spectra of Bi 4f, Ni 2p3/2 and O 1s are analyzed and the results are shown in Fig.3 and S4. Specifically, two Bi 4f peaks, observed at around159.2 eV and 164.5 eV, are characteristic of Bi^{5+} ions, as illustrated in Fig. 3a.[23] Meanwhile, as shown in Fig.S4, Bi can be detected in both surface and bulk. The intensity of Bi on the surface is higher than that at the bulk, indicating that the Bi modification contains both Bi doping and Bi_2O_3 coating. As shown in Fig. 3b, in Ni $2p_{3/2}$ spectra, there are four peaks: the two peaks the Ni^{2+} and Ni^{3+} ions (856 and 854 eV) while the other two are the satellite peaks (861 and 865 eV).[27] According to the Ni 2p3/2 spectrum of VNMC, 1BiNMC, and 3BiNMC, the percentages of Ni^{2+} and Ni^{3+} ions in each sample are calculated. As shown in Fig. 3c and Table S2, 1BiNMC and 3BiNMC contain less Ni^{2+} but more Ni^{3+} ions than VNMC. Especially, the differences of the percentages of Ni^{2+} and Ni^{3+} ions in VNMC and 1BiNMC are obvious. The lower content of Ni^{2+} can be attributed to the similar ionic radii of Bi^{5+} (74Å) and Ni^{2+} (72Å), which allows Bi^{5+} to occupy the sites of Ni^{2+}.[33] Higher content of Ni^{2+} ions can cause higher Li^+/Ni^{2+} disorder in Ni-rich cathode materials, and the cation mixing in VNMC should be higher than that of 1BiNMC, which is corresponding to the result in XRD refinement.

Meanwhile, O1s spectra (Fig. 3d) contain two peaks at 531.9 eV and 529.5 eV. The peak at 531.9 eV represents active oxygen species (Li_2CO_3 and LiOH), while The peak at 529.5 eV is attributed to the lattice oxygen bound to metals. [34] Fig. 3e and Table S4 demonstrate the percentage of the two peaks. 1BiNMC and 3BiNMC have higher content of lattice oxygen bound to metals and less active oxygen species, indicating that the residual lithium can be effectively reduced by Bi_2O_3 coating on the surface and the serious side reaction between

cathode and electrolyte can be limited.[18] As for Co 2p and Mn 2p, their XPS spectra are also carried out and displayed in Fig. S5. There are no obvious position shifts, indicating that the impact of Bi ions on the states of Co and Mn ions is not obvious.

2.3. Electrochemical Performance

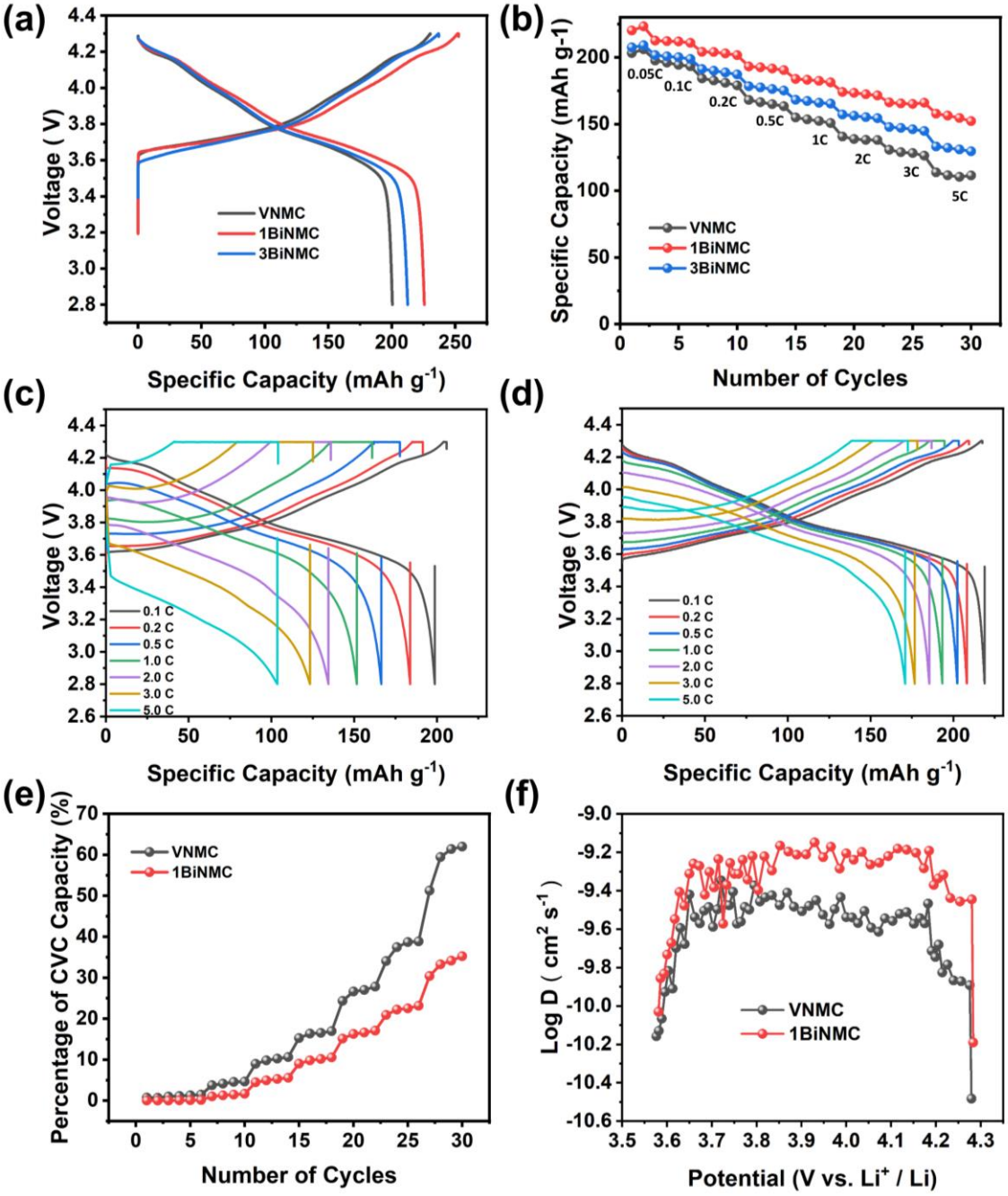

Fig.4. **Rate performance of VNMC, 1BiNMC, and 3BiNMC.** (a) First charge/discharge profiles; (b) rate performance between 2.8 and 4.3 V; (c) the capacity voltage curves with

different current rate of VNMC; (d) the capacity voltage curves with different current rate of 1BiNMC; (e) the percentage of CVC capacity in the total specific charge capacity; (f) Li^+ diffusion coefficients determined through GITT analysis during charge.

The rate performance of VNMC, 1BiNMC, and 3BiNMC is shown in Fig. 4. In Fig. 4a, VNMC delivers an initial charge capacity of 230 $mAhg^{-1}$ and discharge capacity of 204 $mAhg^{-1}$, which is comparable to previous works. [35, 36] When 0.1mol% Bi ions are added, the initial charge and discharge specific capacities of 1BiNMC are 246.1 and 222.9 $mAhg^{-1}$, respectively, which are 16.1 and 18.9 $mAhg^{-1}$ higher than that of VNMC. When the concentration of Bi ions increases to 0.3mol%, the initial charge capacity is 237 $mAhg^{-1}$and discharge specific capacity is 212.5 $mAhg^{-1}$, which are slightly higher than that of VNMC, but lower than that of 1BiNMC.

The same trend can also be observed at different current density. In Fig.4b, VNMC delivers specific rate capacity of 195.35, 181.35, 165.71, 152.88, 138.93,128.53, and 111.83 $mAhg^{-1}$with the current density of 0.1, 0.2, 0.5, 1.0, 2.0, 3.0, and 5.0 C, respectively. For 1BiNMC, it exhibits a specific capacity of 211.88, 203.18, 191.93, 182.67, 172.81, 165.71, and 155.23 $mAhg^{-1}$ from 0.1 to 5.0 C, respectively, which are 16.5 ~ 43.4 $mAhg^{-1}$ higher than VNMC. When the Bi content increases to 0.3 mol%, the specific capacities of 3BiNMC at each current density (200.28, 189.26, 176.81, 166.69, 155.76, 146.46, 131.49 $mAhg^{-1}$) are also larger than that of VNMC, but not as obvious as 1BiNMC. The difference of capacity retention (Fig. S6a) and specific capacity (Fig. 4c, 4d and S6b) among Bi modified samples and VNMC gradually become obvious with the increase of current rate. The variations in specific capacity observed among these samples are primarily attributed to differences in the degree of cation mixing and the lattice parameters of each sample. As indicated in the XRD refinement results, 1BiNMC and 3BiNMC exhibit a lower degree of cation mixing than VNMC, enhancing Li^+ transfer and specific capacity. Meanwhile, the lattice parameter of 1BiNMC and 3BiNMC are larger than

that of VNMC, enabling fast Li^+ diffusion and high specific capacity at high rates. [31] The fast Li^+ diffusion of 1BiNMC also can be contributed by the radial orientation of primary particles because of the short Li^+ diffusion path. Meanwhile, CVC mode is employed to preserve electrochemical equilibrium in the overvoltage state, which occurs due to polarization of the electrodes in the CC mode.[37] The higher percentage of capacity generation in the CVC mode represents the increasing polarization. The CVC capacity and percentage of CVC capacity in total charge capacity are shown in Fig. S6c and Fig. 4e. The percentage of CVC capacity in 1BiNMC is much lower than that in VNMC, indicating the lower polarization of 1BiNMC. Thus, due to the low polarization, 1BiNMC delivers better rate performance than VNMC.

To compare the Li^+ diffusion among VNMC and 1BiNMC, the Li^+ diffusion coefficient (D_{Li}) during charge and discharge process is tested by GITT and CV. As shown in Fig. 4f and Fig. S6d, 1BiNMC delivers higher $D_{Li,}$ than VNMC. Meanwhile, in Fig.S7a and S7b, through a series of CV tests at various scan rates, D_{Li} also can be determined. In Fig.S7c and S7d, the anodic and cathodic slopes corroborate a strong correlation between anodic and cathodic diffusivity, representing the Li^+ diffusion during delithiation and lithiation, respectively.[38] The D_{Li} values of VNMC are calculated to be 2.35×10^{-10} cm^2/s (anodic) and 9.40×10^{-11} cm^2/s (cathodic), which is comparable to previous works.[6] The D_{Li} of 1BiNMC are 6.50×10^{-10} cm^2/s (anodic) and 2.29×10^{-10} cm^2/s (cathodic), which are about 2.8 and 2.4 times higher than the D_{Li} of VNMC, respectively, suggesting that 1BiNMC is able to demonstrate superior electrochemical performance compared to VNMC.

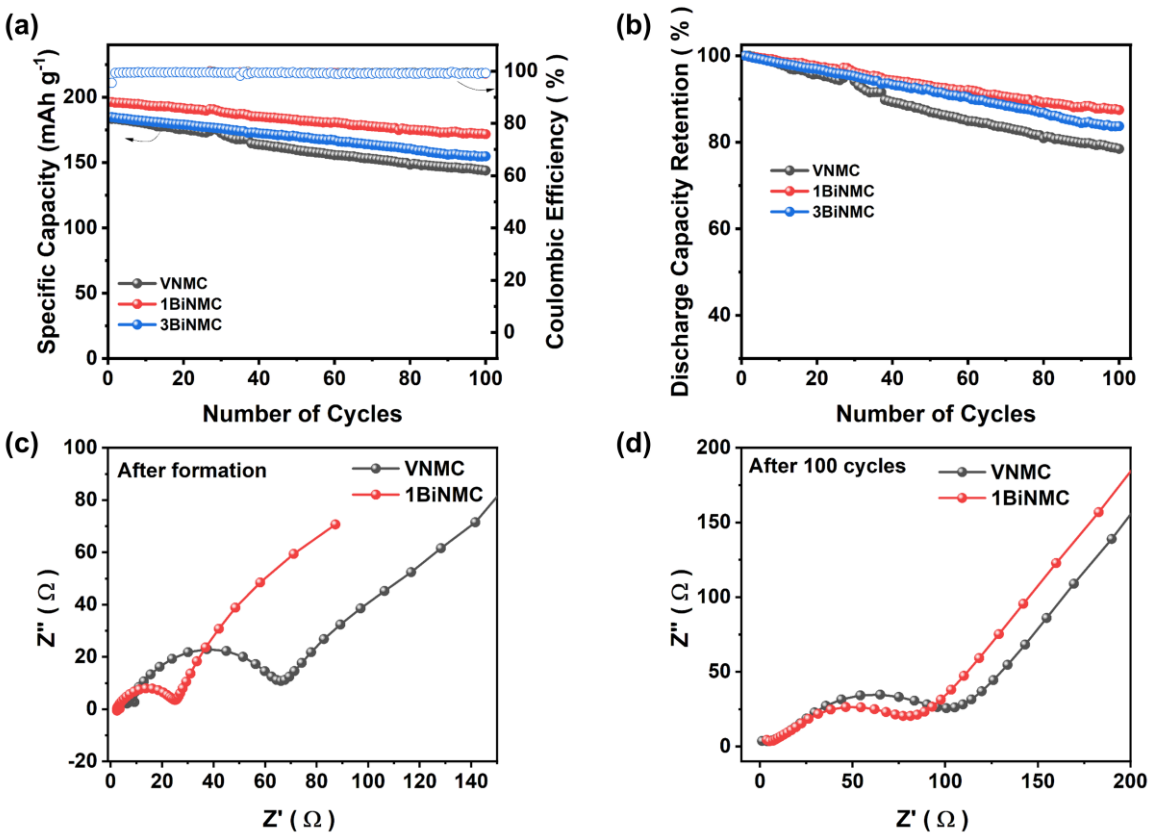

Fig. 5. Cycle performance of VNMC, 1BiNMC, and 3BiNMC. (a) Cycling performances; (b) capacity retention; (c) EIS plots of VNMC and 1BiNMC after formation; (d) EIS plots of VNMC and 1BiNMC after 100 cycles.

The cycling performance of cathode materials is measured with full cells at 0.33 C from 2.5 to 4.2 V (vs. graphite), as shown in Fig. 5a and b. At the 1st cycle with 0.33 C, VNMC delivers a specific discharge capacity of 183.3 $mAhg^{-1}$, and after 100 cycles, the specific capacity drops to 143.9 $mAhg^{-1}$, with a capacity retention of 78.51%. After Bi ions are added, 1BiNMC and 3BiNMC deliver the specific capacity of 196.30 and 184.80 $mAhg^{-1}$ at 1st cycle and a reserved capacity of 171.65 and 154.7 $mAhg^{-1}$ at 100th cycle, respectively. The capacity retention of 1BiNMC and 3BiNMC are 87.44% and 83.71%, respectively. Specifically, 1BiNMC delivers the highest retention capacity after 100 cycles, 27.75 $mAhg^{-1}$higher than VNMC, representing the optimized cycling stability. The enhanced cycle stability of 1BiNMC can be attributed to

its improved structural stability due to its low degree of cation mixing, resulting in the optimized capacity retention during cycling. Meanwhile, the increasing rate of capacity fading is also relevant to the growing cell polarization, which is corresponding to the rise or fall in the median charge or discharge voltage during cycling.[6] The capacity voltage curves of VNMC and 1BiNMC with different cycles are shown in Fig.S8a and b. VNMC exhibits significant voltage attenuation and capacity degradation during cycling, while the voltage attenuation and capacity degradation of 1BiNMC are not such obvious.

To investigate the impact of Bi ions on ionic conduction during cycling, VNMC and 1BiNMC are tested by EIS after formation and cycling (100 cycles). According to the fitted data in Table S4, the Rs values for all the cells remain relatively stable throughout the test duration, demonstrating that the conductivity of electrolyte are not influenced by the Bi ions.[39] However, the difference in the R_{ct} between VNMC and 1BiNMC is obvious. For VNMC, the R_{ct} after formation and after 100 cycles are 7.61 Ω and 61.71 Ω while the R_{ct} of 1BiNMC after formation and after 100 cycles are 3.36 Ω and 47.58, respectively. 1BiNMC exhibits a smaller semicircle (Fig.5c and 5d) and R_{ct} than VNMC, representing the effects of Bi on limiting the charge transfer resistance.

2.4. Degradation analysis

To probe possible degradation mechanisms, the dQ/dV profiles of VNMC and 1BiNMC are presented in Fig. S8c and d, which represent the phase transitions during cycling. At around 4.2V, The phase transition occurring (from H2 to H3 phase) is widely recognized as causing significant lattice shrinkage/expansion along the c-axis, leading to mechanical strain and capacity degradation.[40] The voltage difference of this peak between 1st cycle to 100th cycle for 1BiNMC is 0.21V, which is half of that for VNMC (0.43V), indicating that the characteristic peak indicative the H2 to H3 phase transition of in 1BiNMC exhibits greater reversibility during

cycling. Thus, the mechanical integrity of the particles is preserved, enabling the material to maintain its specific discharge capacity. Meanwhile, this trend also can be found in the results of CV test results. The CV curves of the first 5 cycles are shown in Fig. S9a and b, where the peak-to-peak width of H2 to H3 redox pair increases more rapidly than VNMC, indicating that the irreversibility of the transition in VNMC is faster than that in 1BiNMC.

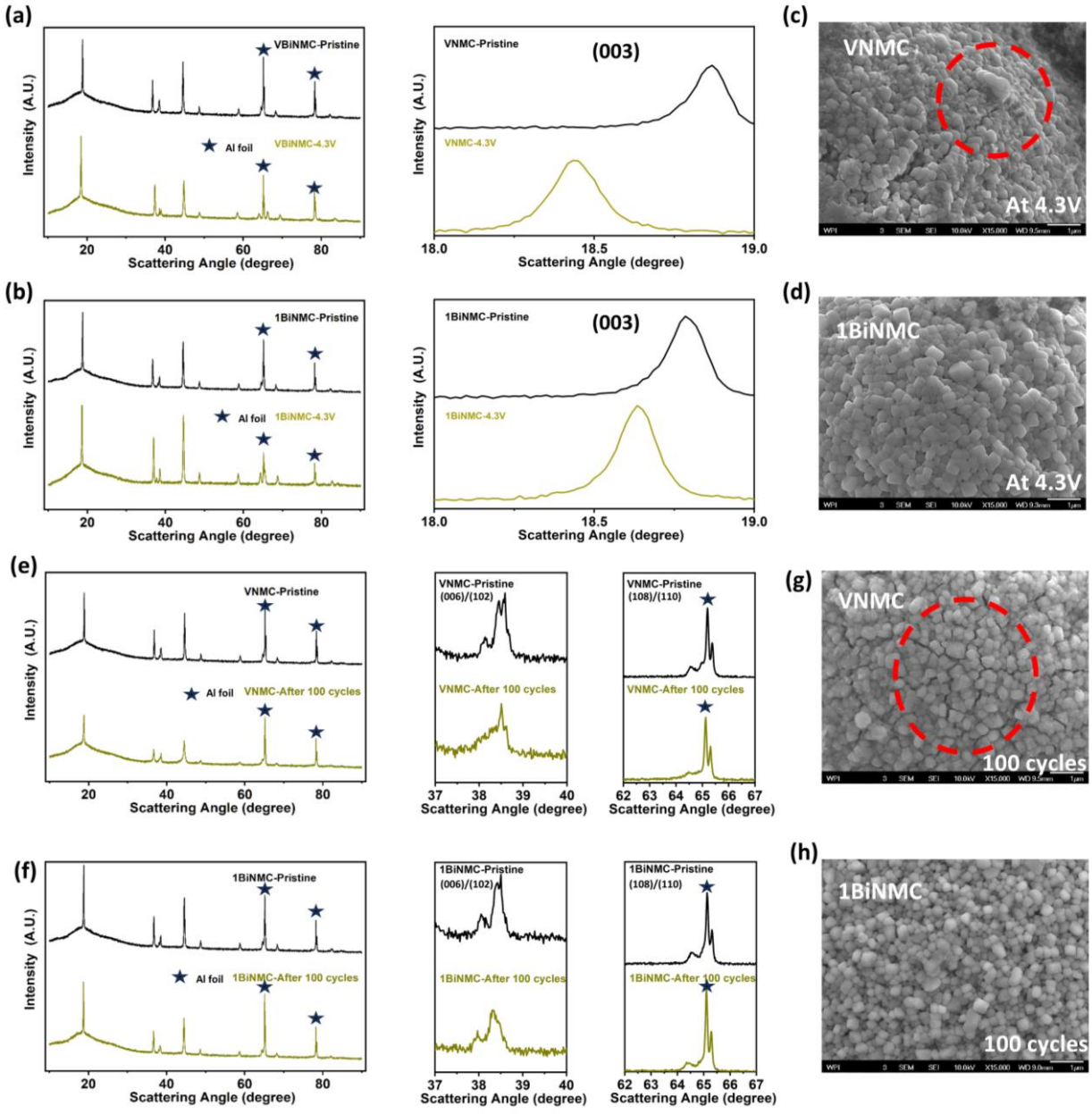

Fig. 6. Ex-situ structural characterizations of VNMC, 1BiNMC, and 3BiNMC. Ex Situ XRD pattern with enlarged (006)/(102) and (108)/(110) peak position of electrodes before and after charging to 4.3V of (a) VNMC and (b) 1BiNMC. SEM images of electrodes charging to 4.3V

of (c) VNMC and (d) 1BiNMC. Ex Situ XRD pattern with enlarged (006)/(102) and (108)/(110) peak position of electrodes before and after 100 cycles of (e) VNMC and (f) 1BiNMC. SEM images of electrodes 100 cycles of (g) VNMC and (h) 1BiNMC.

To further probe the structural change during lithiation/delithiation process, ex situ XRD at 4.3V was performed for both VNMC and 1BiNMC. Typically, the shift in the (003) peak is associated with the intercalation and deintercalation of Li^+ during the lithiation/delithiation process. During charging, Li^+ ions migrate out of the cathode structures towards the anode side, causing the (003) peak shift towards a lower angle. As shown in Fig.6a and b, for 1BiNMC, the (003) peak shift is much smaller than that for VNMC. Since this peak shift is indicative of changes in the c-direction, the smaller shift observed in the 1BiNMC electrode suggests that its crystal structure experiences less contraction in the c-direction.[41, 42] Meanwhile, based on Fig.6c, 6d, S10a, and S10b, even in the first charge process, cracks can be observed in VNMC, while there is no crack in 1BiNMC. Therefore, 1BiNMC possesses a more stable structure than VNMC during lithiation/delithiation process.

The changes in crystal structures of VNMC and 1BiNMC after 100 cycles are also measured by Ex-situ XRD. As displayed in Fig.6e and f, the clearly splitting of (108)/(110) and (006)/(102) peaks of 1BiNMC indicates the well crystalline layered structure after 100 cycles, while due to the unclear splitting of (108)/(110) and unsplit (006)/(102) peaks, VNMC cannot maintain the well crystalline layered structure after 100 cycles. The seriously destroyed layer structure is due to the phase transition from H2 to H3, and the well-maintained layer structure in 1BiNMC is primarily attributed to the stronger TM-O bonds resulting from the substitution of Bi ions into Ni sites, which stabilizes the structure and inhibits the phase transition from H2 to H3 in a highly delithiated state. [15, 17, 43] Moreover, large number of cracks can be found on VNMC after 100 cycles while cracks are hardly observed on 1BiNMC, as shown in Fig.6g, 6h,

S10c, and S10d. The obvious difference also can be attributed to the Bi_2O_3 coating which can effectively prevent limit the corrosion and damage from electrolyte. [18] According to the ex-situ XRD and SEM results, 1BiNMC retains much greater structural crystallinity and morphology after the long cycling than VNMC. According to the results mentioned above, the incorporation of Bi ions can enhance the electrochemical performance of NMC cathode via stabilizing the structure and limiting the contraction in c-direction during lithiation/delithiation process.

3. Conclusion

Bi modified NMC cathodes were successfully synthesized through a facile solid-state reaction from metal oxide, lithium hydroxide and hydroxide precursors. The effects of Bi substitution on the morphology, crystal structure, and electrochemical performance of the NMC cathodes were discovered. It was found that 0.1 mol% Bi substitution(1BiNMC) can significantly improve the rate and cycling performance of unmodified NMC(VNMC). 1BiNMC delivers striking rate capacities, even 43.4 $mAhg^{-1}$ higher than VNMC at 5C. Meanwhile, 1BiNMC provides capacity retention of 87.44% after 100 cycles, ~10% higher than VNMC. The impressive electrochemical performance of the Bi modified NMC cathodes benefits from the role of Bi in improving Li^+ diffusion, structural stability, and cracking resistance during lithiation/delithiation process. Therefore, the effective Bi modification provides a possible solution to optimizing the electrochemical performance of Ni-rich cathodes.

Supporting Information

Supporting Information is available from the Wiley Online Library or from the author.

Acknowledgements

Z. Meng and J. Hou contributed to this work equally. XPS work was conducted at Argonne National Laboratory, and their work was supported by the U.S. Department of Energy, Vehicle Technologies Office, under contract DE-AC02-06CH11357.

Received: ((will be filled in by the editorial staff))
Revised: ((will be filled in by the editorial staff))
Published online: ((will be filled in by the editorial staff))

Reference:

(1) Li, W.; Erickson, E. M.; Manthiram, A. High-nickel layered oxide cathodes for lithium-based automotive batteries. *Nature Energy* **2020**, *5* (1), 26-34. DOI: 10.1038/s41560-019-0513-0.
(2) Liu, Q.; Su, X.; Lei, D.; Qin, Y.; Wen, J.; Guo, F.; Wu, Y. A.; Rong, Y.; Kou, R.; Xiao, X.; et al. Approaching the capacity limit of lithium cobalt oxide in lithium ion batteries via lanthanum and aluminium doping. *Nature Energy* **2018**, *3* (11), 936-943. DOI: 10.1038/s41560-018-0180-6.
(3) Vanaphuti, P.; Liu, Y.; Ma, X.; Fu, J.; Lin, Y.; Wen, J.; Yang, Z.; Wang, Y. Stabilized Lithium, Manganese-Rich Layered Cathode Materials Enabled by Integrating Co-Doping and Nanocoating. *ACS applied materials & interfaces* **2021**, *13* (19), 22597-22607. DOI: 10.1021/acsami.1c04718.
(4) Vanaphuti, P.; Bai, J.; Ma, L.; Ehrlich, S.; Kisslinger, K.; Wang, F.; Wang, Y. Unraveling Na and F coupling effects in stabilizing Li, Mn-rich layered oxide cathodes via local ordering modification. *Energy Storage Materials* **2020**, *31*, 459-469. DOI: https://doi.org/10.1016/j.ensm.2020.08.003.
(5) Manthiram, A.; Goodenough, J. B. Layered lithium cobalt oxide cathodes. *Nature Energy* **2021**, *6* (3), 323-323. DOI: 10.1038/s41560-020-00764-8.
(6) Azhari, L.; Meng, Z.; Yang, Z.; Gao, G.; Han, Y.; Wang, Y. Underlying limitations behind impedance rise and capacity fade of single crystalline Ni-rich cathodes synthesized via a molten-salt route. *Journal of power sources* **2022**, *545*. DOI: 10.1016/j.jpowsour.2022.231963.
(7) Vanaphuti, P.; Cui, Z.; Manthiram, A. Demarcating the Impact of Electrolytes on High-Nickel Cathodes and Lithium-Metal Anode. *Advanced Functional Materials n/a* (n/a), 2308619. DOI: https://doi.org/10.1002/adfm.202308619.
(8) Meng, Z.; Ma, X.; Azhari, L.; Hou, J.; Wang, Y. Morphology controlled performance of ternary layered oxide cathodes. *Communications Materials* **2023**, *4* (1), 90. DOI: 10.1038/s43246-023-00418-8.
(9) Jiang, M.; Danilov, D. L.; Eichel, R. A.; Notten, P. H. A Review of Degradation Mechanisms and Recent Achievements for Ni‐Rich Cathode‐Based Li‐Ion Batteries. *Advanced Energy Materials* **2021**, *11* (48), 2103005.
(10) Ni, L.; Zhang, S.; Di, A.; Deng, W.; Zou, G.; Hou, H.; Ji, X. Challenges and Strategies towards Single-Crystalline Ni-Rich Layered Cathodes. *Advanced Energy Materials* **2022**, *n/a* (n/a), 2201510, https://doi.org/10.1002/aenm.202201510. DOI: https://doi.org/10.1002/aenm.202201510 (acccessed 2022/07/09).
(11) Ryu, H.-H.; Park, K.-J.; Yoon, C. S.; Sun, Y.-K. Capacity Fading of Ni-Rich Li[Ni x Co y Mn1–x–y]O2 (0.6 ≤ x ≤ 0.95) Cathodes for High-Energy-Density Lithium-Ion Batteries: Bulk or Surface Degradation? *Chemistry of materials* **2018**, *30* (3), 1155-1163. DOI: 10.1021/acs.chemmater.7b05269.
(12) Tanim, T. R.; Weddle, P. J.; Yang, Z.; Colclasure, A. M.; Charalambous, H.; Finegan, D. P.; Lu, Y.; Preefer, M.; Kim, S.; Allen, J. M.; et al. Enabling Extreme Fast-Charging: Challenges at the Cathode and Mitigation Strategies. *Advanced Energy Materials* **2022**, *12* (46), 2202795. DOI: https://doi.org/10.1002/aenm.202202795.
(13) Lu, Y.; Zhu, T.; McShane, E.; McCloskey, B. D.; Chen, G. Single-Crystal LiNixMnyCo1−x−yO2 Cathodes for Extreme Fast Charging. *Small* **2022**, *18* (12), 2105833. DOI: https://doi.org/10.1002/smll.202105833.

(14) Thapaliya, B. P.; Misra, S.; Yang, S.-z.; Jafta, C. J.; Meyer III, H. M.; Bagri, P.; Unocic, R. R.; Bridges, C. A.; Dai, S. Enhancing Cycling Stability and Capacity Retention of NMC811 Cathodes by Reengineering Interfaces via Electrochemical Fluorination. *Advanced Materials Interfaces* **2022**, *9* (18), 2200035. DOI: https://doi.org/10.1002/admi.202200035.
(15) Lv, H.; Li, C.; Zhao, Z.; Wu, B.; Mu, D. A review: Modification strategies of nickel-rich layer structure cathode (Ni ≥ 0.8) materials for lithium ion power batteries. *Journal of energy chemistry* **2021**, *60*, 435-450. DOI: 10.1016/j.jechem.2021.01.044.
(16) Qiu, L.; Zhang, M.; Song, Y.; Wu, Z.; Zhu, Y.-F.; Zhang, J.; Wang, D.; Hu, H.-Y.; Li, H.-W.; Liu, H.-R.; et al. Deciphering the degradation discrepancy in Ni-rich cathodes with a diverse proportion of [003] crystallographic textures. *Carbon Energy 5* (7), 298. DOI: https://doi.org/10.1002/cey2.298.
(17) Jiang, Y.; Guo, F.; Qiu, L.; Liu, T.; Hu, Y.; Yang, W.; Liu, Y.; Sun, Y.; Wu, Z.; Song, Y.; et al. Enhancing the Integral Structural and Thermal Stability of Ultrahigh-Ni Cathodes via Morphology Refinement and In Situ Interfacial Engineering. *ACS Applied Materials & Interfaces* **2023**, *15* (29), 35072-35081. DOI: 10.1021/acsami.3c07022.
(18) Liu, Y.; Zeng, T.; Li, G.; Wan, T.; Li, M.; Zhang, X.; Li, M.; Su, M.; Dou, A.; Zeng, W.; et al. The surface double-coupling on single-crystal LiNi0.8Co0.1Mn0.1O2 for inhibiting the formation of intragranular cracks and oxygen vacancies. *Energy Storage Materials* **2022**, *52*, 534-546. DOI: https://doi.org/10.1016/j.ensm.2022.08.026.
(19) Qu, X.; Huang, H.; Wan, T.; Hu, L.; Yu, Z.; Liu, Y.; Dou, A.; Zhou, Y.; Su, M.; Peng, X.; et al. An integrated surface coating strategy to enhance the electrochemical performance of nickel-rich layered cathodes. *Nano Energy* **2022**, *91*, 106665. DOI: https://doi.org/10.1016/j.nanoen.2021.106665.
(20) Yan, W.; Yang, S.; Huang, Y.; Yang, Y.; Guohui, Y. A review on doping/coating of nickel-rich cathode materials for lithium-ion batteries. *Journal of Alloys and Compounds* **2020**, *819*. DOI: 10.1016/j.jallcom.2019.153048.
(21) Ahaliabadeh, Z.; Kong, X.; Fedorovskaya, E.; Kallio, T. Extensive comparison of doping and coating strategies for Ni-rich positive electrode materials. *Journal of Power Sources* **2022**, *540*, 231633. DOI: https://doi.org/10.1016/j.jpowsour.2022.231633.
(22) Zhou, L.; Wu, H.; Tian, M.; Zheng, Q.; Xu, C.; Lin, D. Enhanced cycling stability and rate capability of Bi2O3-coated Li1.2Mn0.54Ni0.13Co0.13O2 cathode materials for lithium-ion batteries. *RSC advances* **2016**, *6* (74), 6979-69797. DOI: 10.1039/c6ra14087d.
(23) Hao, Y.; Liu, W.; Zhang, Q.; Wang, X.; Yang, H.; Kou, L.; Tian, Z.; Shao, L.; Maleki Kheimeh Sari, H.; Wang, J.; et al. Optimized activation of Li2MnO3 effectively boosting rate capability of xLi2MnO3·(1-x)LiMO2 cathode. *Nano Energy* **2021**, *88*, 106240. DOI: https://doi.org/10.1016/j.nanoen.2021.106240.
(24) Zhang, S.; Hu, G.; Du, K.; Peng, Z.; Li, L.; Zhang, Y.; Cao, Y. Enhanced cycle performance and synthesis of LiNi0.6Co0.2Mn0.2O2 single-crystal through the assist of Bi ion. *Electrochimica Acta* **2023**, *470*, 143280. DOI: https://doi.org/10.1016/j.electacta.2023.143280.
(25) Zhou, Y.; Zhang, H.; Wang, Y.; Wan, T.; Guan, P.; Zhou, X.; Wang, X.; Chen, Y.; Shi, H.; Dou, A.; et al. Relieving Stress Concentration through Anion–Cation Codoping toward Highly Stable Nickel-Rich Cathode. *ACS Nano* **2023**, *17* (20), 20621-20633. DOI: 10.1021/acsnano.3c07655.
(26) Liang, J.; Lu, Y.; Wang, J.; Liu, X.; Chen, K.; Ji, W.; Zhu, Y.; Wang, D. Well-ordered layered LiNi0.8Co0.1Mn0.1O2 submicron sphere with fast electrochemical kinetics for cathodic lithium storage. *Journal of Energy Chemistry* **2020**, *47*, 188-195. DOI: https://doi.org/10.1016/j.jechem.2019.12.009.
(27) Zhang, R.; Meng, Z.; Ma, X.; Chen, M.; Chen, B.; Zheng, Y.; Yao, Z.; Vanaphuti, P.; Bong, S.; Yang, Z.; et al. Understanding fundamental effects of Cu impurity in different forms

for recovered LiNi0.6Co0.2Mn0.2O2 cathode materials. *Nano Energy* **2020**, *78*, 105214. DOI: https://doi.org/10.1016/j.nanoen.2020.105214.
(28) Wan, C.; Zhao, L.; Wu, C.; Lin, L.; Liu, X. Bi5+ doping improves the electrochemical properties of Ti/SnO2–Sb/PbO2 electrode and its electrocatalytic performance for phenol. *Journal of Cleaner Production* **2022**, *380*, 135005. DOI: https://doi.org/10.1016/j.jclepro.2022.135005.
(29) Ma, X.; Vanaphuti, P.; Fu, J.; Hou, J.; Liu, Y.; Zhang, R.; Bong, S.; Yao, Z.; Yang, Z.; Wang, Y. A universal etching method for synthesizing high-performance single crystal cathode materials. *Nano Energy* **2021**, *87*. DOI: 10.1016/j.nanoen.2021.106194.
(30) Wang, J.; Liu, C.; Xu, G.; Miao, C.; Wen, M.; Xu, M.; Wang, C.; Xiao, W. Strengthened the structural stability of in-situ F− doping Ni-rich LiNi0.8Co0.15Al0.05O2 cathode materials for lithium-ion batteries. *Chemical engineering journal (Lausanne, Switzerland : 1996)* **2022**, *438*, 135537. DOI: 10.1016/j.cej.2022.135537.
(31) Li, F.; Liu, Z.; Shen, J.; Xu, X.; Zeng, L.; Zhang, B.; Zhu, H.; Liu, Q.; Liu, J.; Zhu, M. A nanorod-like Ni-rich layered cathode with enhanced Li+ diffusion pathways for high-performance lithium-ion batteries. *Journal of Materials Chemistry A* **2021**, *9* (5), 2830-2839. DOI: 10.1039/d0ta10608a.
(32) Mao, G.; Luo, J.; Zhou, Q.; Xiao, F.; Tang, R.; Li, J.; Zeng, L.; Wang, Y. Improved cycling stability of high nickel cathode material for lithium ion battery through Al- and Ti-based dual modification. *Nanoscale* **2021**, *13* (44), 18741-18753, 10.1039/D1NR06005H. DOI: 10.1039/D1NR06005H.
(33) Sathishkumar, G.; Venkataraju, C.; Murugaraj, R.; Sivakumar, K. Bismuth effect in the structural, magnetic and dielectric properties of CoZn ferrite. *Journal of Materials Science: Materials in Electronics* **2012**, *23* (1), 243-250. DOI: 10.1007/s10854-011-0395-9.
(34) Liu, Y.; Tang, L.-b.; Wei, H.-x.; Zhang, X.-h.; He, Z.-j.; Li, Y.-j.; Zheng, J.-c. Enhancement on structural stability of Ni-rich cathode materials by in-situ fabricating dual-modified layer for lithium-ion batteries. *Nano Energy* **2019**, *65*. DOI: 10.1016/j.nanoen.2019.104043.
(35) Wu, H.; Pang, X.; Bi, J.; Wang, L.; Li, Z.; Guo, L.; Liu, H.; Meng, Q.; Jiang, H.; Liu, C.; et al. Cellulose nanofiber assisted hydrothermal synthesis of Ni-rich cathode materials with high binding particles for lithium-ion batteries. *Journal of alloys and compounds* **2020**, *829*, 154571. DOI: 10.1016/j.jallcom.2020.154571.
(36) Zhang, M.; Wang, C.; Zhang, J.; Li, G.; Gu, L. Preparation and Electrochemical Characterization of La and Al Co-doped NCM811 Cathode Materials. *ACS Omega* **2021**, *6* (25), 16465-16471. DOI: 10.1021/acsomega.1c01552.
(37) Lee, Y.; Park, C.; Park, K. Elucidating the Relationship between Quality Control of the Coating Layer and Suppression of Gas Evolution in Li-Ion Batteries. *Chemistry of Materials* **2024**, *36* (1), 232-246. DOI: 10.1021/acs.chemmater.3c01998.
(38) Zheng, Y.; Zhang, R.; Vanaphuti, P.; Liu, Y.; Yang, Z.; Wang, Y. Positive Role of Fluorine Impurity in Recovered LiNi0.6Co0.2Mn0.2O2 Cathode Materials. *ACS Applied Materials & Interfaces* **2021**, *13* (48), 57171-57181. DOI: 10.1021/acsami.1c17341.
(39) Thanwisai, P.; Vanaphuti, P.; Yao, Z.; Hou, J.; Meng, Z.; Ma, X.; Guo, H.; Gao, G.; Yang, Z.; Wang, Y. Regulating Anionic Redox via Mg Substitution in Mn-Rich Layered Oxide Cathodes Enabling High Electrochemical Stability for Sodium-Ion Batteries. *Small n/a* (n/a), 2306465. DOI: https://doi.org/10.1002/smll.202306465.
(40) Li, Q.; Dang, R.; Chen, M.; Lee, Y.; Hu, Z.; Xiao, X. Synthesis Method for Long Cycle Life Lithium-Ion Cathode Material: Nickel-Rich Core–Shell LiNi0.8Co0.1Mn0.1O2. *ACS Applied Materials & Interfaces* **2018**, *10* (21), 17850-17860. DOI: 10.1021/acsami.8b02000.
(41) Li, J.; Shunmugasundaram, R.; Doig, R.; Dahn, J. R. In Situ X-ray Diffraction Study of Layered Li–Ni–Mn–Co Oxides: Effect of Particle Size and Structural Stability of Core–Shell

Materials. *Chemistry of materials* **2016**, *28* (1), 162-171. DOI: 10.1021/acs.chemmater.5b03500.
(42) Qiu, L.; Xiang, W.; Tian, W.; Xu, C.-L.; Li, Y.-C.; Wu, Z.-G.; Chen, T.-R.; Jia, K.; Wang, D.; He, F.-R.; et al. Polyanion and cation co-doping stabilized Ni-rich Ni–Co–Al material as cathode with enhanced electrochemical performance for Li-ion battery. *Nano energy* **2019**, *63*, 103818. DOI: 10.1016/j.nanoen.2019.06.014.
(43) Qiu, L.; Song, Y.; Zhang, M.; Liu, Y.; Yang, Z.; Wu, Z.; Zhang, H.; Xiang, W.; Liu, Y.; Wang, G.; et al. Structural Reconstruction Driven by Oxygen Vacancies in Layered Ni-Rich Cathodes. *Advanced Energy Materials* **2022**, *12* (19), 2200022. DOI: https://doi.org/10.1002/aenm.202200022.

Table of contents

Understanding the Effects of Bi Modification on the Properties of Ni-rich Cathodes

Z. Meng, J. Hou, P. Thanwisai, J. Fu, Z. Yao, Y. Zheng, W. Jin, Z. Wang, Z. Yang, X. Ma, Y. Wang.
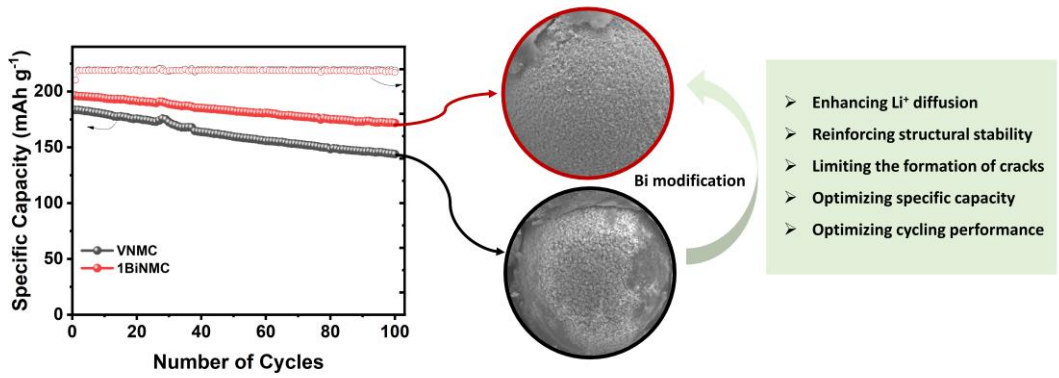
The figure shows cycle performance of 1BiNMC and VNMC. At 0.33C, 1BiNMC delivers higher specific capacity (196.3 $mAhg^{-1}$) than VNMC (183.3 $mAhg^{-1}$). Meanwhile, the capacity retention of 1BiNMC is higher than VNMC after 100 cycles at 0.33C. The optimized electrochemical performance of 1BiNMC is due to the enhanced Li^+ diffusion, reinforced structural stability and less formation of cracks.